Electronic Supplementary Material (ESI) for Journal of Materials Chemistry A.

Supporting information

B←N bonds alter the photo-generated electron/hole separation ability of conjugated polymers to promote photocatalytic performance

Peiyan Chen, [a] Fanbo Ji, [b] Detian Ma, [a] Yangbin Xie, [a] Xuan Wu, [a] Mingcai Zhang, [a] Chenglong Ru, *, [a] Lian Zhou, *, [c] Jincai Wu, [a] Xiaobo Pan *, [a, c]

a. State Key Laboratory of Applied Organic Chemistry (Lanzhou University), Key Laboratory of Nonferrous Metal Chemistry and Resources Utilization of Gansu Province, College of Chemistry and Chemical Engineering, Lanzhou University, Lanzhou 730000, People's Republic of China, E-mail: boxb@lzu.edu.cn (Xiaobo Pan) and ruchl18@lzu.edu.cn (Chenglong Ru).

b. School of Physical Science & Technology, Lanzhou University, Lanzhou 730000, People's Republic of China.

c. New Energy (Photovoltaic) Industry Research Centre, Qinghai University, Xining 810006, People's Republic of China, Email: zhoulianminai@126.com (Lian Zhou).

Corresponding Author

Xiaobo Pan, E-mail: boxb@lzu.edu.cn; Chenglong Ru, Email: ruchl18@lzu.edu.cn; Lian Zhou, Email: zhoulianminai@126.com.

General Methods

All reactions and manipulations are carried out under an argon atmosphere by using the bubbling method or standard Schlenk techniques or an inter-atmosphere glovebox. Prior to use CH_2Cl_2, and toluene were dried by refluxing and degassed by applying two freeze-pump-thaw cycles. All chemicals (reagents and solvents) were obtained from commercial suppliers (Energy Chemical, BidePharm) and directly used without further purification.

Instrumentations

The Fourier transform infrared (FT-IR) spectra of the samples were recorded with a Bruker Vertex 70 with a spectral range of 4000-400 cm^{-1} using the KBr disk method. The ^{1}H NMR spectrums were performed using a JEOL JNM-ECS-400 at room temperature. Solid ^{13}C CP/MAS NMR and ^{11}B CP/MAS NMR spectrums were performed using Bruker-AVANCE II 400MHz. The surface morphologies of the polymers were acquired by scanning electron microscopy (SEM) on a Hitachi-S4800, Japan, operating at 5 kV. Powder X-ray diffraction (PXRD) patterns were measured using X-ray diffraction (PANALYTICAL-X'pert pro and Rigaku Corporation-MiniFlex600) equipped with Cu Kα radiation (λ = 1.54056 Å) at the scattering angle 2θ between 3-50°. UV-visible diffuse reflectance spectrums were recorded at room temperature on Agilent Carry 5000 UV-Vis-NIR spectrometer. Photoluminescence spectroscopy was collected with a photoluminescence spectrophotometer Edinburgh FLS920 at room temperature. Time-correlated single-photon counting (TCSPC) experiments were performed on an Edinburgh FLS920 fluorescence spectrophotometer with picosecond pulsed LED excitation sources and an R928 detector. Decay times were fitted in the F900 software using suggested lifetime estimates. Zeta potential was performed on Malvern nano-zs. Transient photocurrent responses and electrochemical impedance spectra wre recorded using a CHI-760E electrochemical workstation in a standard three-electrode configuration. A 300 W Xenon lamp equipped with an AM 1.5G filter (100 mW cm^{-1}) was used as the light source in the photocurrent response measurement. The analysis of X-ray photoelectron spectra (XPS) was performed by a multifunctional photoelectron spectrometer-ESCALAB XI+ from Thermo Fisher. The molecular surface electrostatic potential was determined by an atomic force microscope equipped with a Kelvin probe (KPFM, MultiMode 8 of Bruker). Electron Paramagnetic Resonance (EPR) testing was done on ER200DSRC10/12 of Bruker. Transient photovoltage (TPV) was carried out using CEL-SPS1000 (Beijing China Education Au-Light Technology). The transmission electron microscope (TEM) is carried by Tecnai F30 Transmission Electron Microscope.

Photocatalytic hydrogen production experiment

The testing conditions for photocatalytic activity are as follows: A flask is charged with the polymer powder, a 1:1:1 vol. mixture of water, triethylamine, and methanol (50 mL). The resulting suspension is ultrasonicated until the photocatalyst is dispersed before degassing by N_2 bubbling for 30 min. The accumulated amount of evolved gases is monitored every 60 min using a gas chromatograph (Yidian Analysis GC126N) equipped with a thermal conductive detector (TCD). The light source is a 300 W Xe lamp with an AM 1.5G filter applied to simulate sunlight (100 mW cm^{-1}). Hydrogen is detected with a TCD detector, referencing standard gases with known concentrations of hydrogen.

Loading Pt experiment

6 mg of catalyst is added to a photocatalytic bottle containing mixture solvent (V_{H20}: V_{MeOH}: V_{TEA} = 1: 1: 1), followed by the corresponding amount of chloroplatinic acid (e.g., 1% Pt: 16 μL, 8 mg ml^{-1} of chloroplatinic acid). The photocatalyst is ultrasonicated for 20 min to evenly distribute the photocatalyst in the solvent and then deoxygenated by nitrogen bubbling for 30 min. Afterward, photo-deposition of loaded Pt is carried out under AM 1.5G simulated sunlight irradiation.

Apparent quantum yield measurements

The apparent quantum yield (AQY) for H_2 evolution was measured using monochromatic visible 420 nm, 450 nm, 500 and 550 nm. The AQY was calculated as the following equation:

$$AQY = \frac{N_e}{N_p} \times 100\%$$
$$= \frac{2 \times M \times N_A}{E_{total}/E_{photon}} \times 100\%$$
$$= \frac{2 \times M \times N_A}{(S \times P \times t)/\left(h \times \frac{c}{\lambda}\right)} \times 100\%$$
$$= \frac{2 \times M \times N_A \times h \times c}{S \times P \times t \times \lambda} \times 100\%$$

Where, M was the amount of H_2 (mol), N_A was Avogadro constant (6.022×10^{23} /mol), h was the Planck constant (6.626×10^{-34} J·s), c was the speed of light (3×10^{8} m/s), S was the irradiation area (cm^2), P was the intensity of irradiation light (W/cm^2), t was the photoreaction time (s), λ was the wavelength of the monochromatic light (m).

Experimental Section

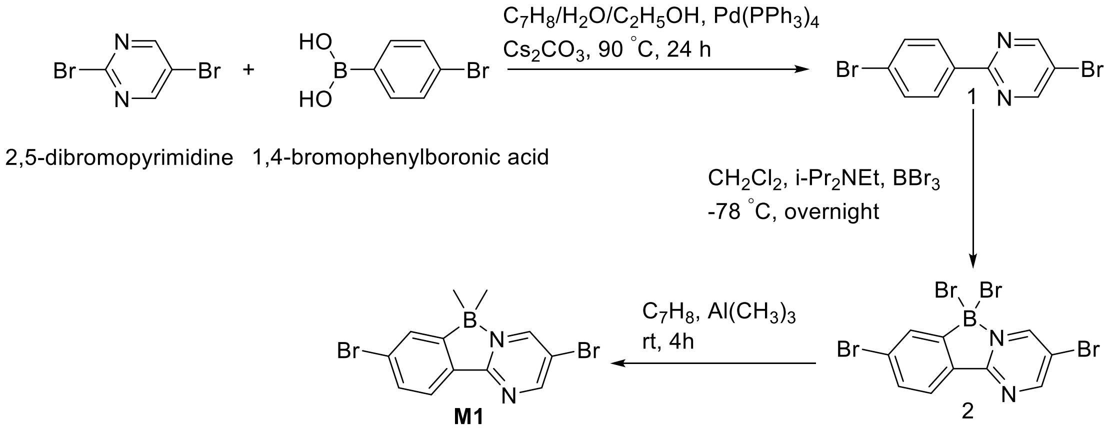

Scheme S1 The synthetic procedures of **M1**.

The synthetic procedures the **Monomer 1** (**M1**):

Compound 1: Under argon atmosphere, deoxidizing mixed solvent (39 mL C_7H_8, 26 mL distilled water and 13 mL C_2H_5OH) was added to a 100 mL branch flask containing 2, 5-dibromopyrimidine (4.53 g, 19.04 mmol), 1,4-bromophenylboronic acid (3.23 g, 16.08 mmol), Cs_2CO_3 (16.9 g, 51.87 mmol) and $Pd(PPh_3)_4$ (0.23 g,0.20 mmol). The system was heated to 90 °C and stirred for 24 h. After the reaction was completed, 100 mL water was added to quench the reaction. It was extracted with ethyl acetate (3 x 100 mL), combined with the organic phase, dried with anhydrous magnesium sulfate, and steamed to obtain the crude product. The crude product was separated by silica gel chromatography column ($V_{\text{petroleum ether}}$: $V_{\text{dichloride}}$ = 1:1), and after drying at 60 °C overnight, 4.54 g white solid product was obtained (90% yield). ^1H NMR (400 MHz, $CDCl_3$): δ 8.82 (s, 2H), 8.29 (d, J = 8.5 Hz, 2H), 7.62 (d, J = 10.9 Hz, 2H).

Compound 2: Under argon atmosphere, compound 1 (3.00 g, 9.55 mmol), 1.4 mL of diisopropylethylamine (i-Pr_2NEt) and 50 mL of deoxygenated dry dichloromethane solvent were added to a 100 mL flask and the reaction system was cooled to -78 °C. 29 mL of BBr_3 (1.0 mol/L) was added and the solution changed from white to yellow, then the temperature of the system was gradually brought to room temperature and the reaction was carried out overnight. The next day, 50 mL of water was added for quenching, and the precipitate was washed with 300 mL of acetone and dried in a vacuum oven at 60 °C overnight to obtain the crude product 3.01 g.

M1: Under argon atmosphere, trimethylaluminum (8.54 ml, 1.6 mol/L) was added into a 100 mL flask containing 60 mL C_7H_8 and the crude product of compound 2 (3.01 g, < 6.20 mmol), and the solution changes from turbid to clear. After 4 h, 100 mL of water was added to quench the reaction, and the reaction was carried out with ethyl acetate (3 × 100 mL). The organic phase was combined, dried with anhydrous magnesium sulfate, and the crude product was obtained by spin evaporation. The crude product was separated by silica gel column ($V_{\text{petroleum ether}}$: $V_{\text{dichloride}}$ = 1:1). After drying in a vacuum oven at 60 °C overnight, a white solid product of 0.80 g (24% overall yield) was obtained. ^{1}H NMR (400 MHz, $CDCl_3$): δ 9.01 (d, *J* = 2.5 Hz, 1H), 8.66 (d, *J* = 2.4 Hz, 1H), 7.98 (d, *J* = 8.2 Hz, 1H), 7.75 (s, 1H), 7.48 (dd, *J* = 8.2, 1.6 Hz, 1H), 0.05 (s, 6H); ^{13}C NMR (101 MHz, $CDCl_3$): δ 162.72, 161.46, 150.61, 132.19, 131.93, 129.31, 128.92, 125.45, 114.89, 8.09.

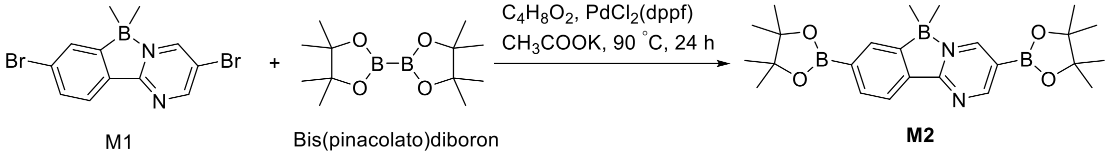

Scheme S2 The synthetic procedures of **M2**.

Monomer 2 (**M2**): Under argon atmosphere, 25 mL deoxygenated dry $C_4H_8O_2$ was added to a 100 mL flask containing monomer M1 (0.60 g, 1.70 mmol), boronic acid pinacol ester (1.33 g, 5.24 mmol), potassium acetate (1.00 g, 13.60 mmol) and $PdCl_2$(dppf) (0.06 g, 0.08 mmol). The system was heated to 90 °C and maintained for 24 h. After the reaction was completed, 100 mL of water was added to quench the reaction and extracted with ethyl acetate (3 × 100 mL), and the organic phase was combined, dried over anhydrous magnesium sulfate, and the crude product was obtained by spin evaporation. The crude product was separated by silica gel column ($V_{\text{petroleum ether}}$: $V_{\text{dichloride}}$ = 1:3) and dried in a vacuum oven at 60 °C overnight to obtain 0.67 g of white solid product (88% yield). ^{1}H NMR (400 MHz, $CDCl_3$): δ 9.22 (d, J = 1.9 Hz, 1H), 8.87 (d, J = 1.9 Hz, 1H), 8.19 (d, J = 7.7 Hz, 1H), 8.13 (s, 1H), 7.81 (d, J = 7.6 Hz, 1H), 1.39 (d, J = 7.4 Hz, 24H), 0.07 (s, 6H); ^{13}C NMR (101 MHz, $CDCl_3$): δ 166.17, 165.85, 155.15, 136.66, 135.57, 132.04, 123.33, 85.18, 83.84, 24.93, 24.82, 8.36.

The typical procedure of Suzuki-Miyaura coupling polymerization:

A flask was equipped with the monomers, $Pd(PPh_3)_4$ and K_2CO_3. The mixture solvent of water and DMF was degassed by bubbling method for 30 min. The reaction was heated to 100 °C for 2 days. The mixture was cooled to room temperature and poured into water. The precipitate was collected by filtration and washed with H_2O, methanol, acetone and chloroform. Further purification was performed by Soxhlet extraction with methanol and THF for 1 day.

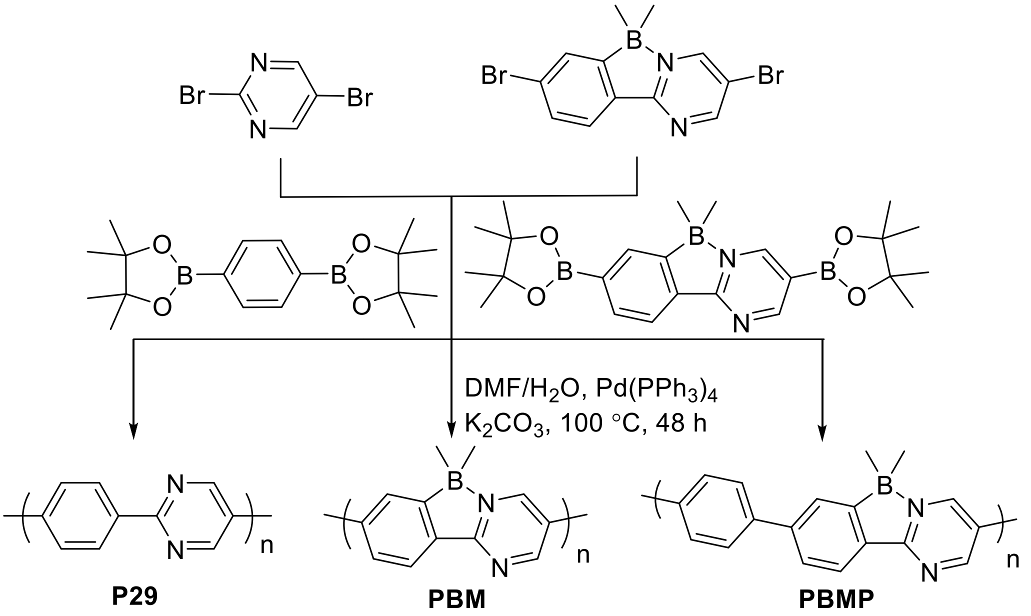

Scheme S3 The synthetic procedures of the conjugated polymers.

Synthesis of P29: 1,4-benzenediboronic acid bis(pinacol) ester (330 mg, 1 mmol), 2, 5-dibromo pyrimidine (238 mg, 1 mmol), tetrakis(triphenylphosphine palladium) (40 mg), dimethylformamide (30 mL) and potassium carbonate (2 M, 6 mL) was used. After the work-up, the product obtained after drying was a gray-green solid (121 mg, 80% yield).

Synthesis of PBM: M2 (448 mg, 1 mmol), M1 (354 mg, 1 mmol), tetrakis(triphenylphosphine palladium) (40 mg), dimethylformamide (30 mL) and potassium carbonate (2 M, 6 mL) was used. After the work-up, the product obtained after drying was a yellow solid (309 mg, 79% yield).

Synthesis of PBMP: 1,4-benzenediboronic acid bis(pinacol) ester (330 mg, 1 mmol), M1 (354 mg, 1 mmol), tetrakis(triphenylphosphine palladium) (40 mg), dimethylformamide (30 mL) and potassium carbonate (2 M, 6 mL) was used. After the work-up, the product obtained after drying was a green solid (242 mg, 89% yield).

DFT calculation

All density functional theory calculations were performed using Gaussian 09 program package. The structure of **M29**, **MBM** and **MBMP** were all optimized by B3LYP with 6-311G (d, p). CAM-B3LYP/6-311G (d, p) was used for the calculation of S_0 and S_1 dipole moments in the ground state structure. MESP was calculated by Multiwfn. For hydrogenation, the geometry optimizations and frequency calculations (**MBM-C1-H, MBM-C2-H and MBM-N1-H**) were carried out with the B3LYP hybrid functional and 6-31G (d, p) basis set while the electronic total energies were computed with additional single-point correction at the M06-2x/6-311++G (d, p) theory level. Induced current visualization was done with the help of POV software.

Other characterization charts

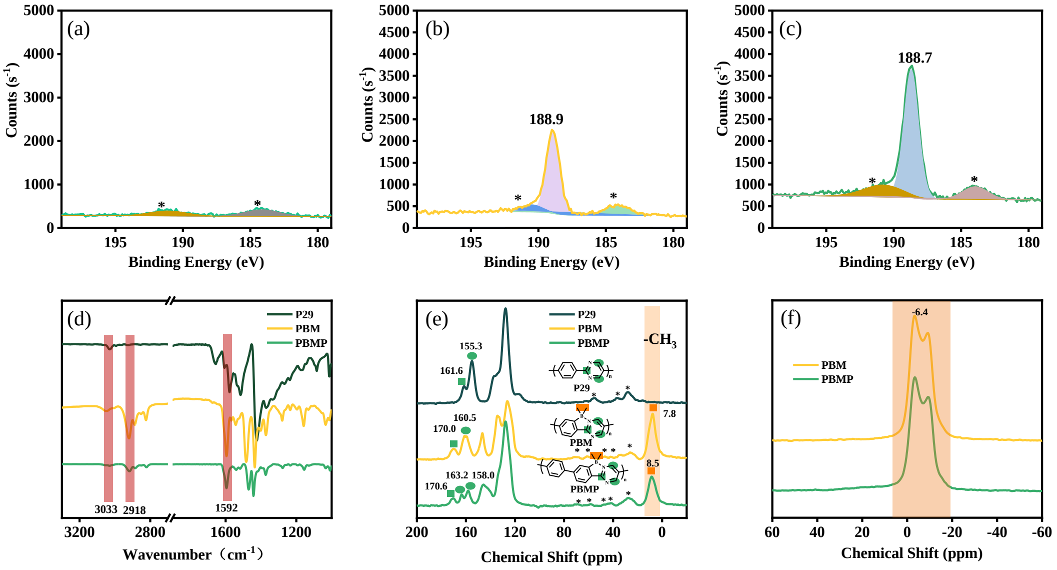

Figure S1 XPS B 1s of three conjugated polymers (* represents the outgoing peak of the end group Br and Bpin). (a) **P29**. (b) **PBM**. (c) **PBMP**. (d) FT-IR of the conjugated polymers. (e) ^{13}C CP/MAS NMR of the conjugated polymers (* is the sideband signal). (f) ^{11}B CP/MAS NMR of **PBM** and **PBMP**.

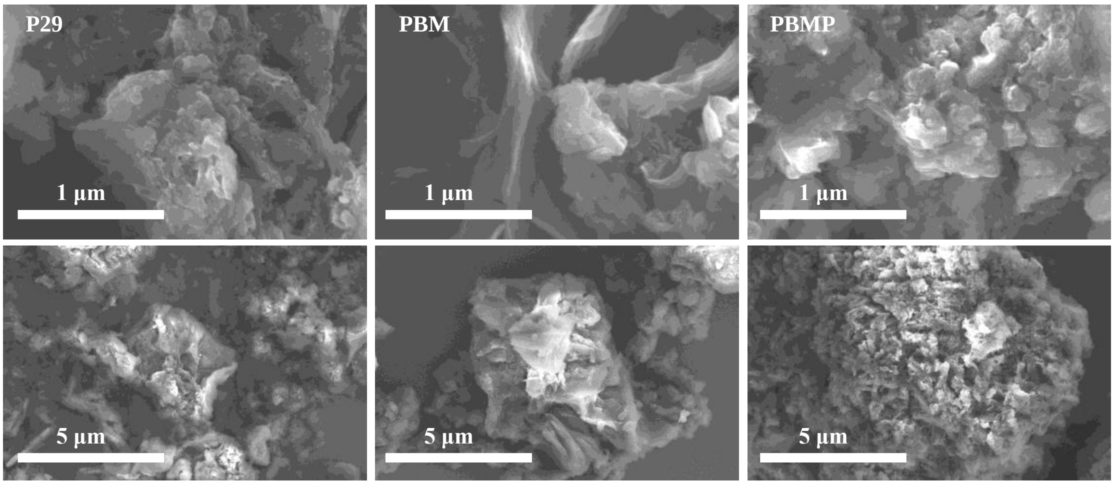

Figure S2 Morphology of three conjugated polymers at different microscopic scales taken by SEM.

The morphologies of the conjugated polymer are photographed at the scale of 1 μm as well as 5 μm. The results show that all conjugated polymers are disordered block stacks.

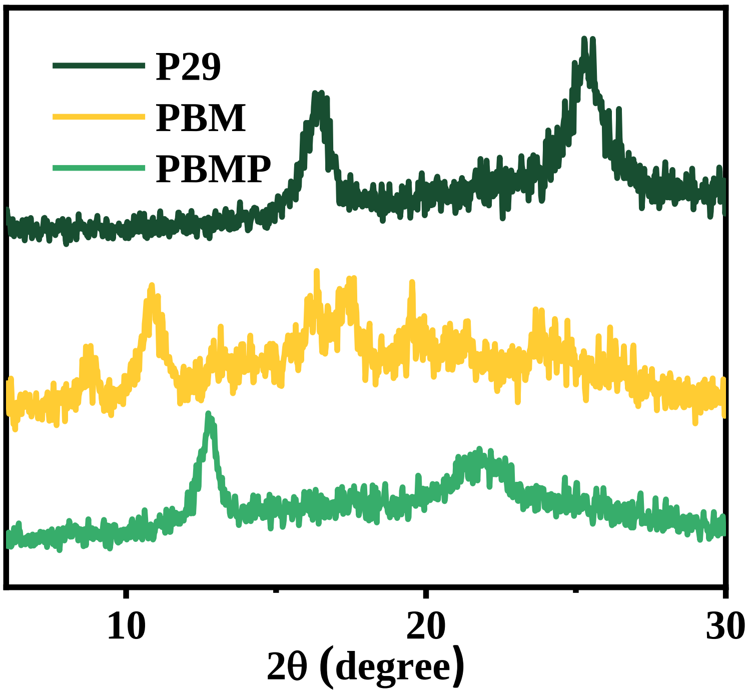

Figure S3 PXRD of polymers **P29**, **PBM**, and **PBMP**.

PXRD of the three conjugated polymers is obtained at a sweep rate of 5° per minute. The results show that all three conjugated polymers are semi-crystalline. The peaks of **P29** are mainly at 16.4° and 25.3°, with a new peak at 10.9° after the introduction of B←N bonds. This indicated that the introduction of B←N bonds probably changed the stacking of the conjugated polymers.

Good crystallinity implies that the ordered stacking of polymers will facilitate intermolecular charge transfer and thus enhance the HERs. However, PXRD tests show that all three conjugated polymers are semi-crystalline with disordered stacking, and thus the stacking pattern might not be the main reason for the enhanced photocatalytic activity in this manuscript (*J. Mater. Chem. A*, 2022, **10**, 17691-17698; *Angew. Chem.*

Int. Ed., 2016, **55**, 9202).

Table S1 The calculation related to dipole moments of **M29**, **MBM** and **MBMP**.

Compounds	x	y	z	Total	$\Delta\mu_{ge}$
M29	0	0	1.76	1.76	
M29 (TD)	0	0	-0.12	0.12	1.88
MBM	-3.45	-1.75	0	3.86	
MBM (TD)	1.69	-1.19	0	2.07	5.17
MBMP	-3.35	-1.56	-0.16	3.70	
MBMP (TD)	3.02	-1.63	-0.21	3.44	6.37

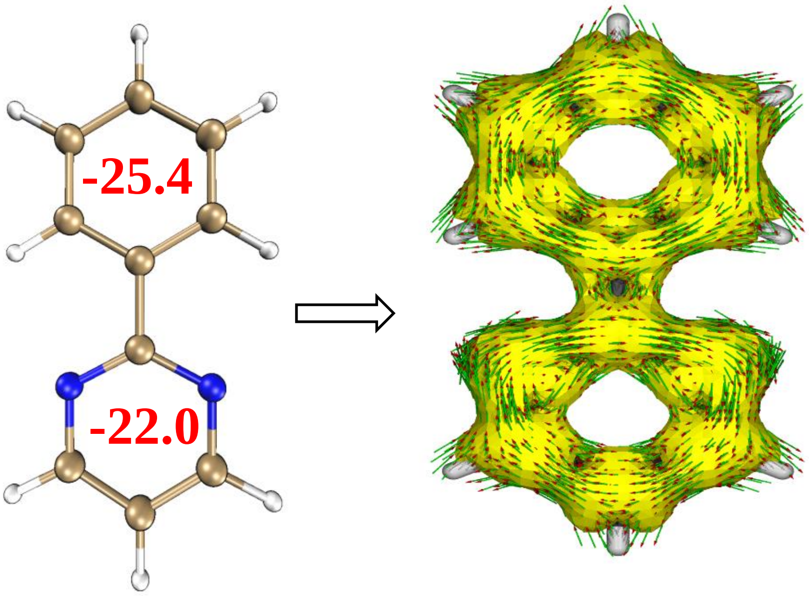

M29

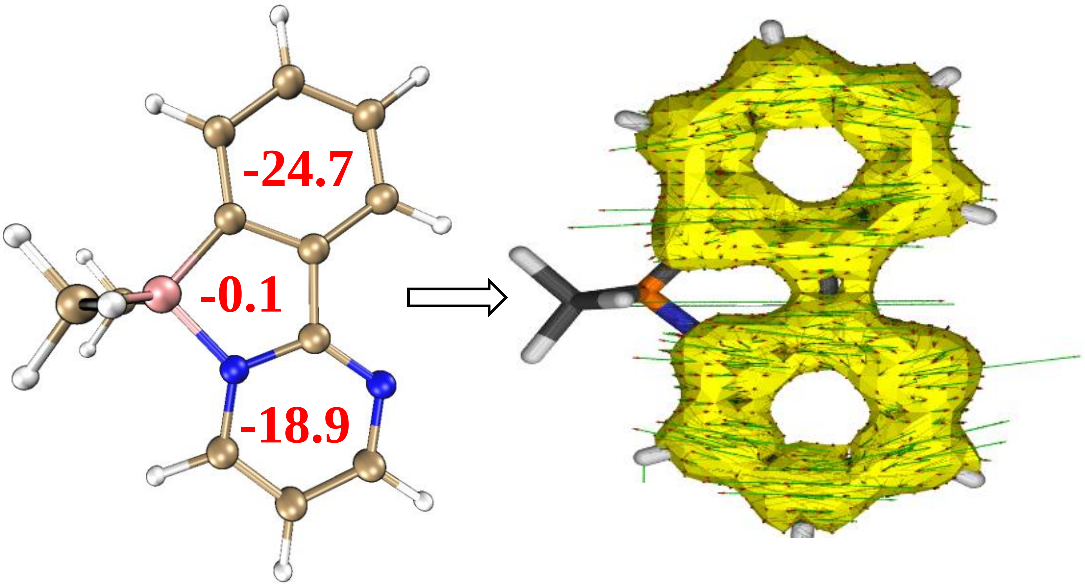

MBM

Figure S4 The NICSzz values of each ring of **M29** and **MBM** and induced currents of the corresponding rings.

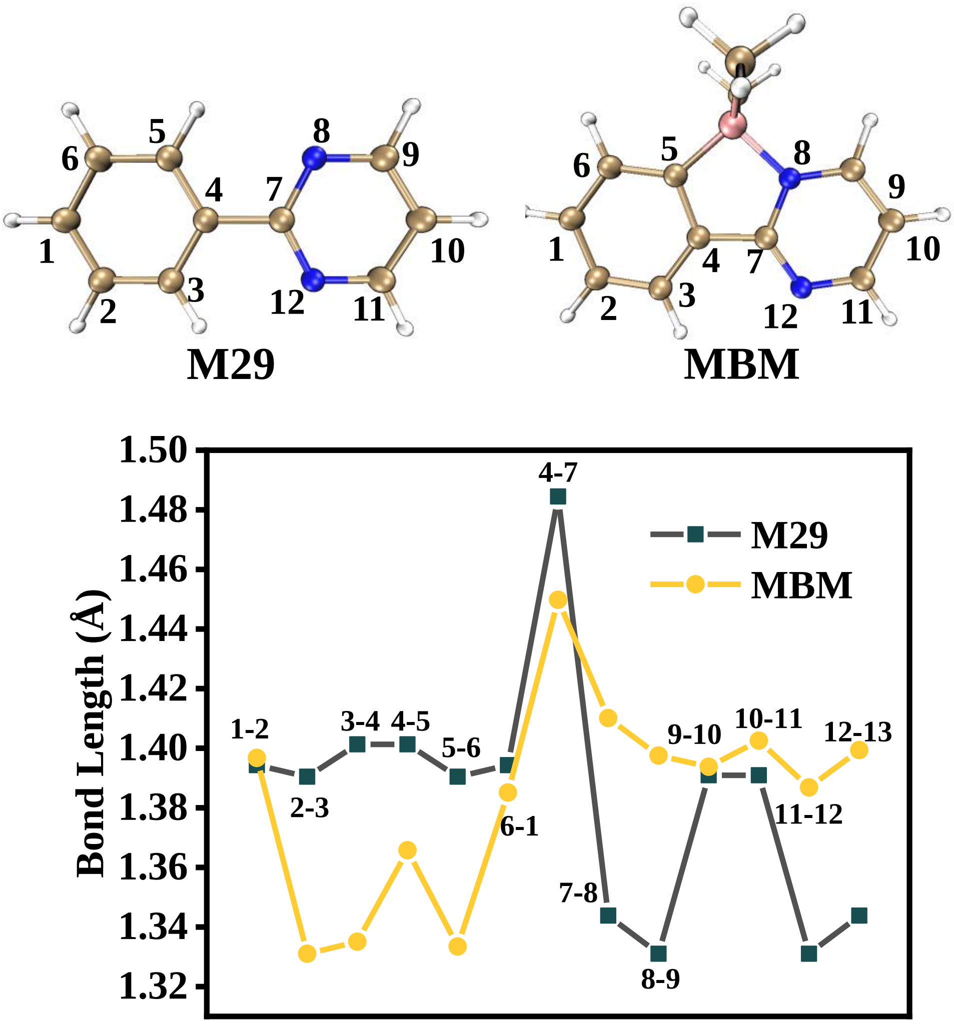

Figure S5 The bond length of benzene and pyrimidine of **M29** and **MBM**.

A possible link between bond length changes and photocatalytic activity: There is a close relationship between the change in bond length and photocatalytic performance. Firstly, the bond length is affected by electron cloud density, and the change in bond length also means a change in electronic structure. For **M29** and **MBM**, the introduction of B←N bonds with large dipole moments (5.2 D) affects the positive and negative potential distribution of the skeleton, thus giving the conjugated skeleton a strong electron push-pull effect, and the bond length changes accordingly. Strong electron push-pull effects often imply excellent photocatalytic activity (*Acc. Chem. Res.*, 2020, **53**, 1557-1567; *Macromolecules*, 2021, **54**, 6718-6725). In addition, bond lengths also affect intramolecular charge transfer (*Nat. Commun.*, 2021, **12**, 6335). **M29** has poor charge transport and the electrons and holes are mainly distributed on the pyrimidine ring. The bond length of **MBM** is greatly changed after the introduction of B←N bonds. The electrons and holes are better separated and the corresponding charge transfer ability is improved.

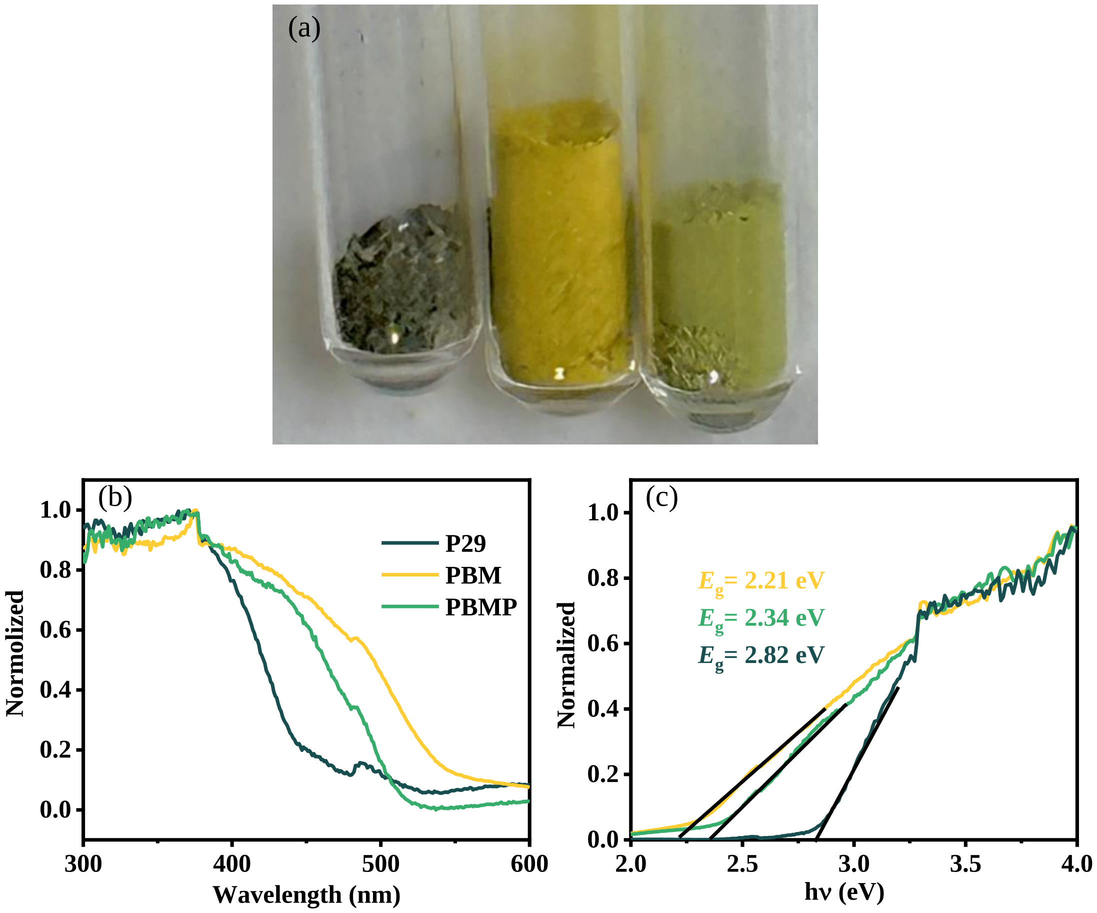

Figure S6 P29, **PBM**, and **PBMP** (a) Solid powder images. (b) UV-vis DRS. (c) Optical bandgap obtained from tauc plot.

About the direct or indirect bandgap: The general method of determining the direct or indirect bandgap is the semiconductor electron jumps with (without) releasing or absorbing phonons (i.e., lattice vibrations). Direct bandgap semiconductors do not require the release or absorption of phonons for electron jumps, whereas indirect bandgap semiconductors do. In our manuscript, the backbone of conjugated polymer is comprised of a linear series of overlapping pz orbitals that have formed via sp2 hybridization, thereby creating a conjugated chain of delocalized electron density. In the research of photocatalytic hydrogen production for conjugated polymer, the primary photo-excitations in the conjugated skeleton are bound electron-hole pairs (excitons) rather than free charge carriers; this is largely due to their low dielectric constant and the presence of significant electron-lattice interactions and electron correlation effects. In the absence of a mechanism to dissociate the excitons into free charge carriers, the exciton will undergo radiative and nonradiative decay, with a typical exciton lifetime in the range from 100 ps to 1 ns (*Chem. Rev.*, 2010, **110**, 6736-6767). Therefore, the polymers in this paper belong to the direct bandgap (*ACS Catal.*, 2019, **9**, 9438-9445; *Chem. Sci.*, 2021, **12**, 1796-1802).

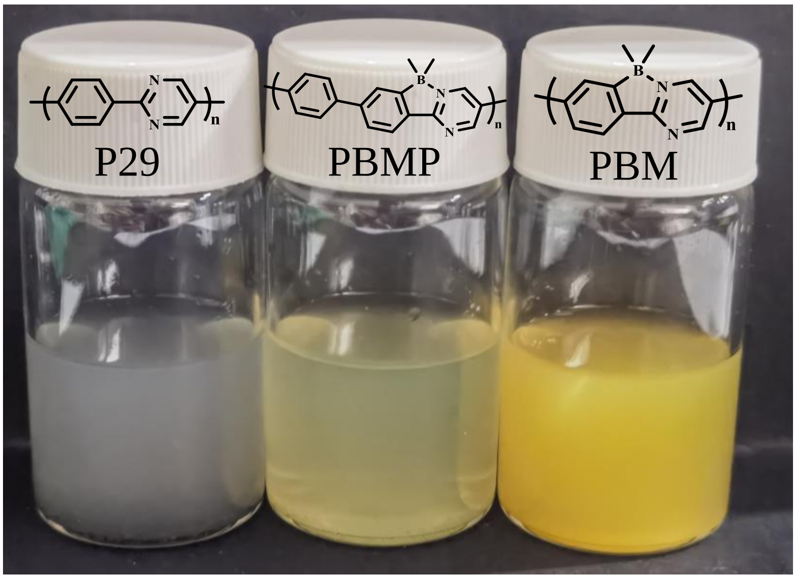

Figure S7 Pictures of three conjugated polymers dispersed in methanol.

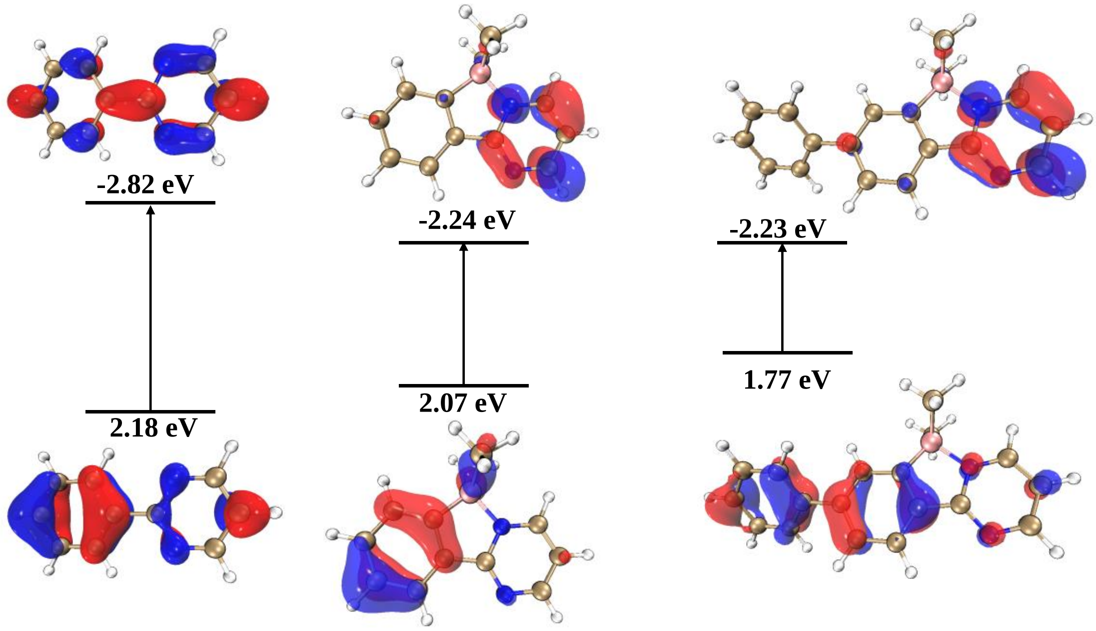

Figure S8 Distribution of HOMO (positive) and LUMO level (negative) and frontier orbits for **M29**, **MBM** and **MBMP**.

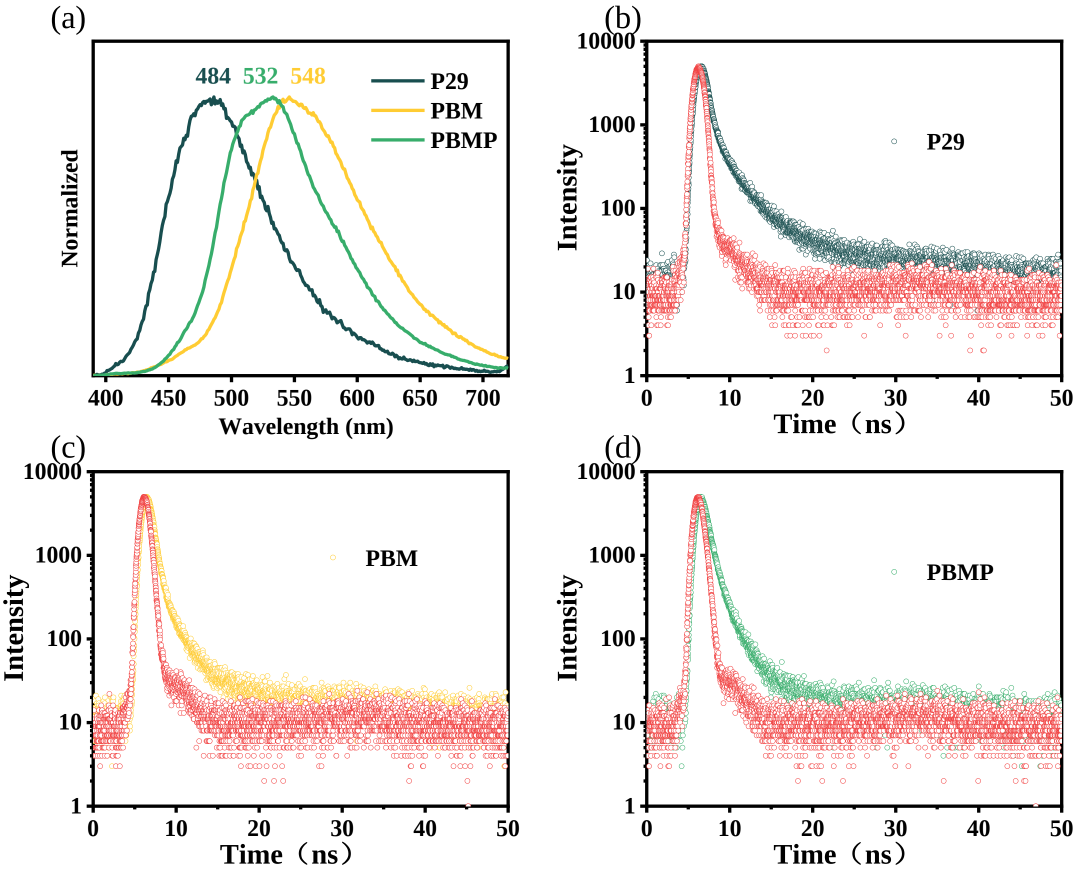

Figure S9 **P29**, **PBM** and **PBMP** of (a) emission peak under 360 nm excitation. (b-d) TCSPCs are obtained under the conditions of optimal emission and 360 nm excitation.

Table S2 TCSPC of the polymers in the solid state.

Samples	**P29**	**PBM**	**PBMP**
Emission (nm)	483	548	532
τ_1 (ns)	0.29	0.27	0.12
B_1	0.037	0.039	0.070
τ_2 (ns)	1.64	1.07	1.03
B_2	0.003	0.004	0.006
τ_3 (ns)	6.12	4.54	3.32
B_3	0	0	0
χ^2	1.11	1.04	1.08
τ_{AV} (ns)	0.71	0.50	0.50

Excitation wavelength λ_{ex} = 360 nm.

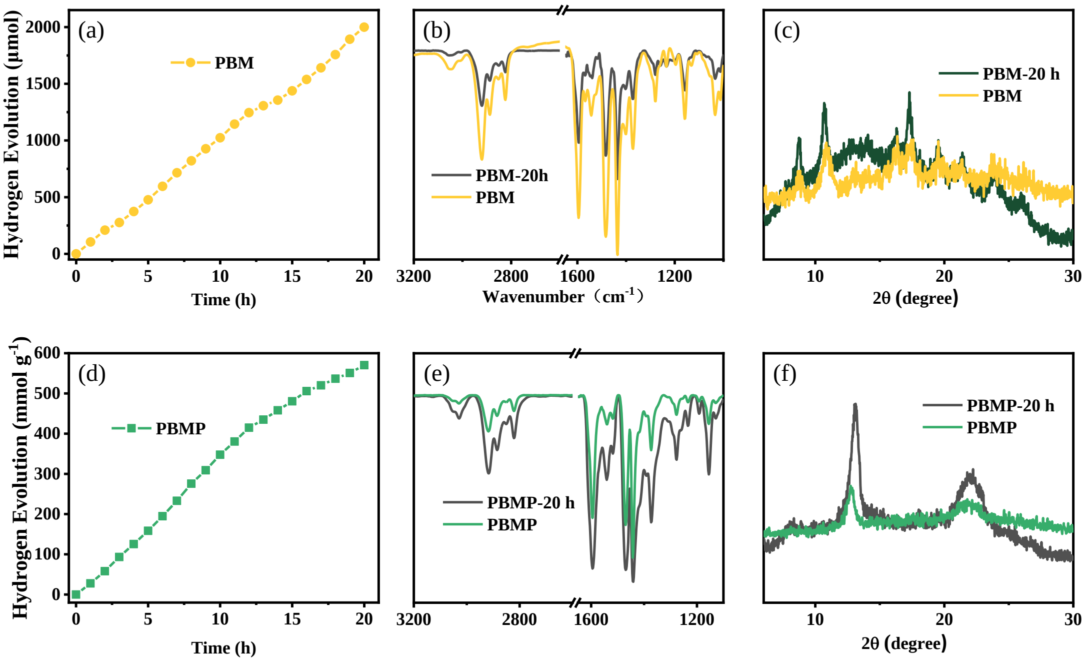

Figure S10 From left to right: cumulative hydrogen production by during 20 h continuous light irradiation, the FT-IR and PXRD before and after 20 h. (a-c) **PBM**. (d-f) **PBMP**.

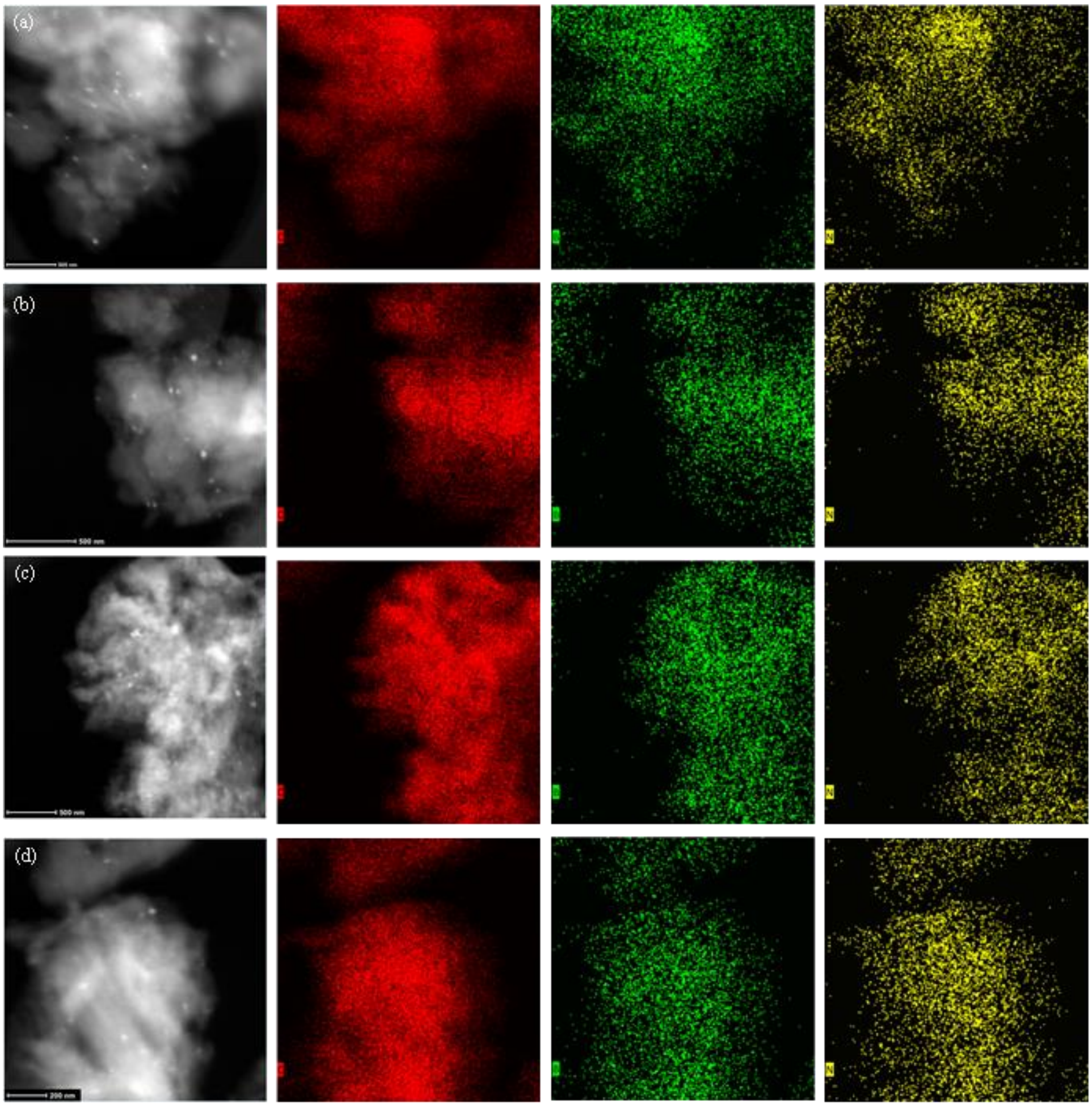

Figure S11 From left to right: typical TEM image, elemental mappings for C, B and N.

(a) **PBM** (b) **PBM-20 h** (c) **PBMP** (d) **PBMP-20 h**.

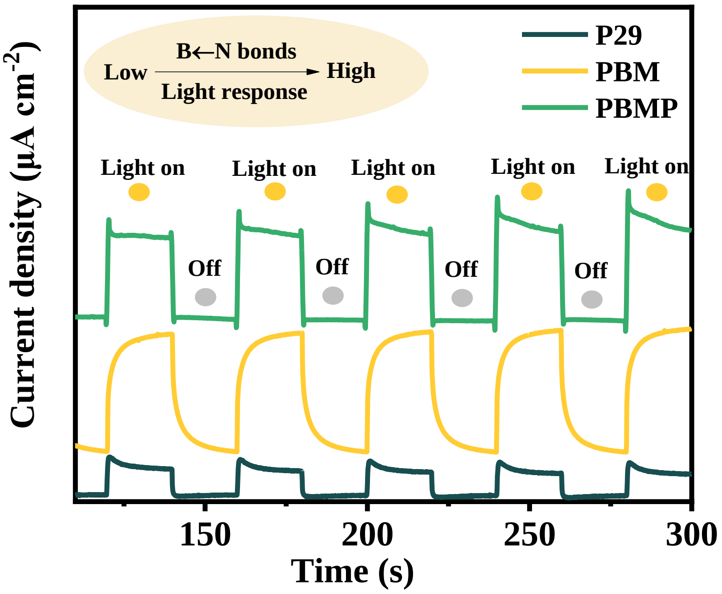

Figure S12 Photocurrent of three conjugated polymers under AM 1.5 G simulated sunlight irradiation (100 mW cm^{-2}).

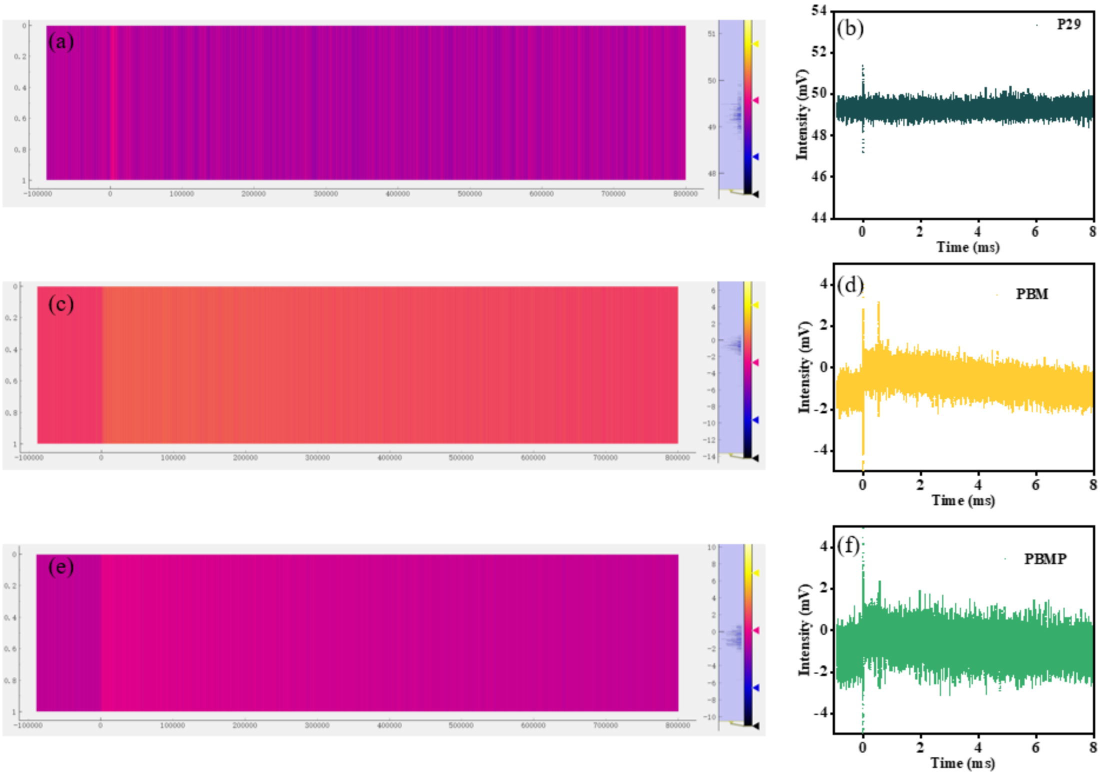

Figure S13 TPV test of (a-b) **P29**. (c-d) **PBM**. (e-f) **PBMP**.

Table S3 Contribution of each non-hydrogen atom to electron and hole of **M29**.

M29	Hole	Electron	Overlap	Difference
1C	6.16%	1.35%	2.89%	-4.81%
2C	3.67%	29.62%	10.42%	25.95%
3C	8.12%	1.33%	3.28%	-6.79%
4N	36.40%	18.33%	25.83%	-18.07%
5C	3.67%	29.62%	10.42%	25.95%
6C	-1.39%	0.03%	0	1.42%
7C	0.72%	0.18%	0.36%	-0.54%
8C	0.72%	0.18%	0.36%	-0.54%
9C	0.04%	0.21%	0.09%	0.16%
10C	0.04%	-0.07%	0	-0.11%
11C	0.04%	0.21%	0.09%	0.16%
12N	36.40%	18.33%	25.83%	-18.07%

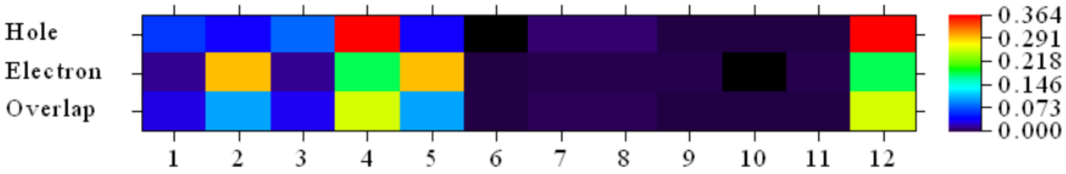

Figure S14 Heat map representation of the contribution of each non-hydrogen atom to the electron and hole of **M29**.

Table S4 Contribution of molecular orbitals (MOs) to electron and hole of **M29**.

M29	Hole	Electron
MO39 (HOMO-2)	98.71%	0
MO43 (LUMO+1)	0	97.32%
MO44 (LUMO+2)	0	1.68%

Table S5 Contribution of each non-hydrogen atom to hole and electron of **MBM**.

MBM	Hole	Electron	Overlap	Difference
1C	7.35%	7.95%	7.64%	0.60%
2C	0.39%	19.43%	2.77%	19.03%
3C	0.66%	19.42%	3.57%	18.76%
4N	2.78%	17.40%	6.96%	14.62%
5C	1.71%	6.29%	3.28%	4.58%
6C	18.51%	2.41%	6.67%	-16.11%
7C	21.16%	5.49%	10.78%	-15.68%
8B	1.86%	0.57%	1.03%	-1.29%
9C	2.29%	6.18%	3.76%	3.89%
10C	18.00%	0.79%	3.77%	-17.21%
11C	7.19%	7.77%	7.47%	0.58%
12C	5.62%	1.48%	2.88%	-4.14%
13C	2.63%	1.03%	1.65%	-1.60%
14C	2.63%	1.03%	1.65%	-1.60%
15N	5.64%	1.48%	2.89%	-4.17%

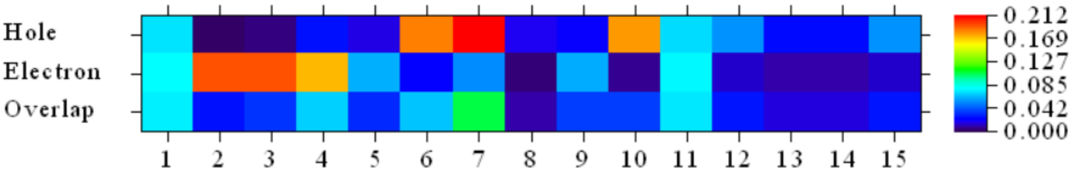

Figure S15 Heat map representation of the contribution of each non-hydrogen atom to the electron and hole of **MBM**.

Table S6 Contribution of MOs to the electron and hole of **MBM**.

MBM	Hole	Electron
MO47 (HOMO-4)	1.72%	0
MO51 (HOMO-1)	8.29%	0
MO52 (HOMO)	88.55%	0
MO53 (LUMO)	0	86.91%
MO54 (LUMO+1)	0	9.71%
MO55 (LUMO+2)	0	1.70%

Table S7 Contribution of each non-hydrogen atom to hole and electron of **MBMP**.

MBMP	Hole	Electron	Overlap	Difference
1C	7.93%	8.56%	8.24%	0.62%
2C	0.31%	16.19%	2.25%	15.88%
3C	0.65%	19.36%	3.54%	18.71%
4N	3.70%	15.56%	7.59%	11.86%
5C	1.27%	3.96%	2.24%	2.70%
6C	23.54%	2.91%	8.28%	-20.62
7C	12.26%	5.39%	8.13%	-6.87%
8B	0.70%	0.49%	0.58%	-0.22%
9C	1.05%	6.27%	2.57%	5.22%
10C	14.17%	0.75%	3.26%	-13.42
11C	11.59%	8.65%	10.01%	-2.94%
12C	0.56%	2.21%	1.11%	1.65%
13C	0.86%	0.97%	0.91%	0.11%
14C	0.65%	0.97%	0.79%	0.31%
15N	6.05%	0.64%	1.97%	-5.41%
16C	2.91%	1.47%	2.07%	-1.43%
17C	0.48%	0.16%	0.28%	-0.32%
18C	3.90%	1.64%	2.53%	-2.25%
19C	0.43%	0.20%	0.30%	-0.23%
20C	2.96%	1.37%	2.02%	-1.59%
21C	3.22%	1.03%	1.82%	-2.19%

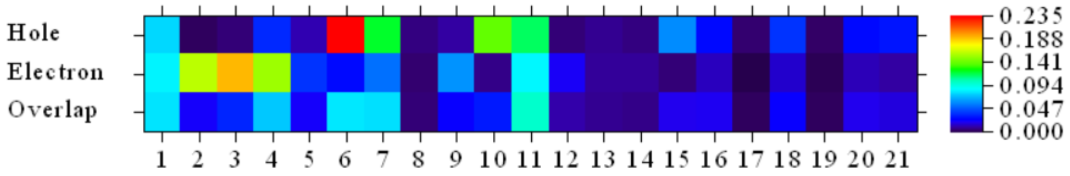

Figure S16 Heat map representation of the contribution of each non-hydrogen atom to the electron and hole of **MBMP**.

Table S8 Contribution of MOs to the electron and hole of **MBMP**.

MBMP	Hole	Electron
MO69 (HOMO-2)	6.16%	0
MO71 (HOMO-1)	10.95%	0
MO72 (HOMO)	80.19%	0
MO73 (LUMO)	0	94.93%
MO74 (LUMO+1)	0	1.99%
MO75 (LUMO+2)	0	1.07%

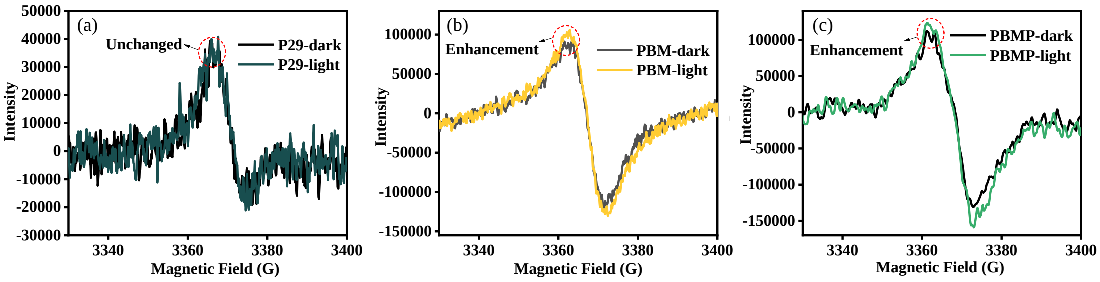

Figure S17 EPR signal changes of (a) **P29** (b) **PBM** (c) and **PBMP** in dark and light.

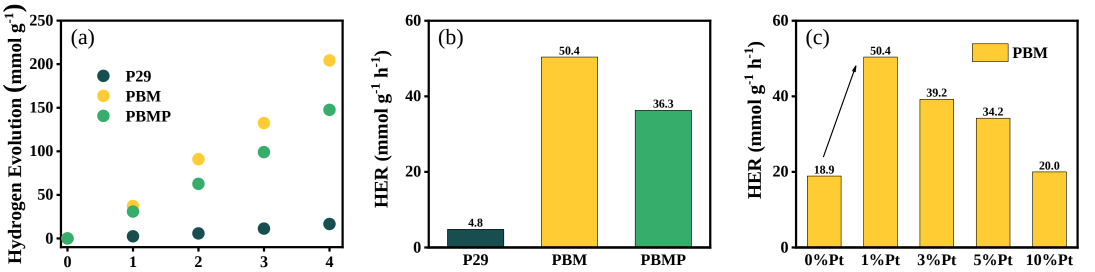

Figure S18 (a) Hydrogen production-time diagram for **P29**, **PBM** and **PBMP** and (b) HERs for three conjugated polymers loaded with 1% Pt (c) HERs of **PBM** corresponding to different loadings of Pt.

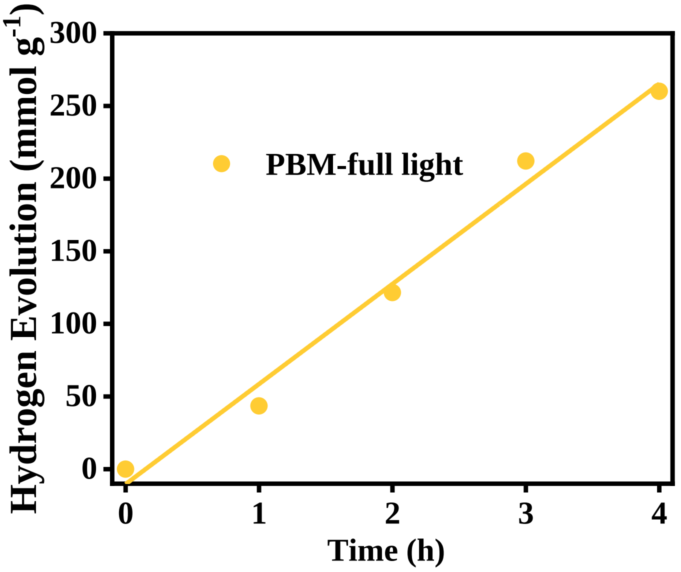

Figure S19 HERs of **PBM** under full light irradiation (100 mW cm^{-2}).

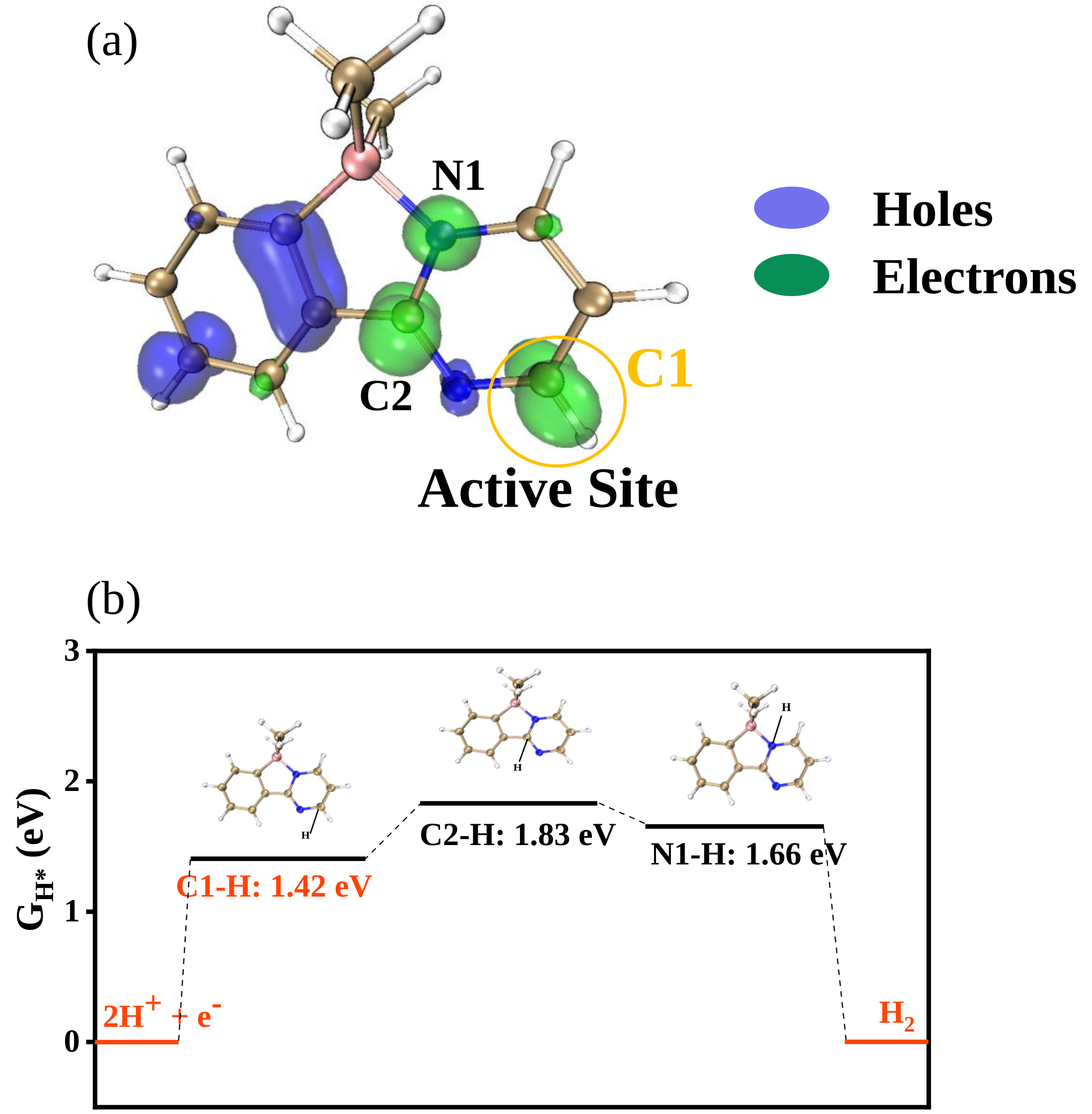

Figure S20 MBM of (a) the difference of electron density before and after excitation (blue represents the decrease of electron cloud density, green represents the increase of electron density cloud). (b) The change of Gibbs free energy after hydrogenation at different sites.

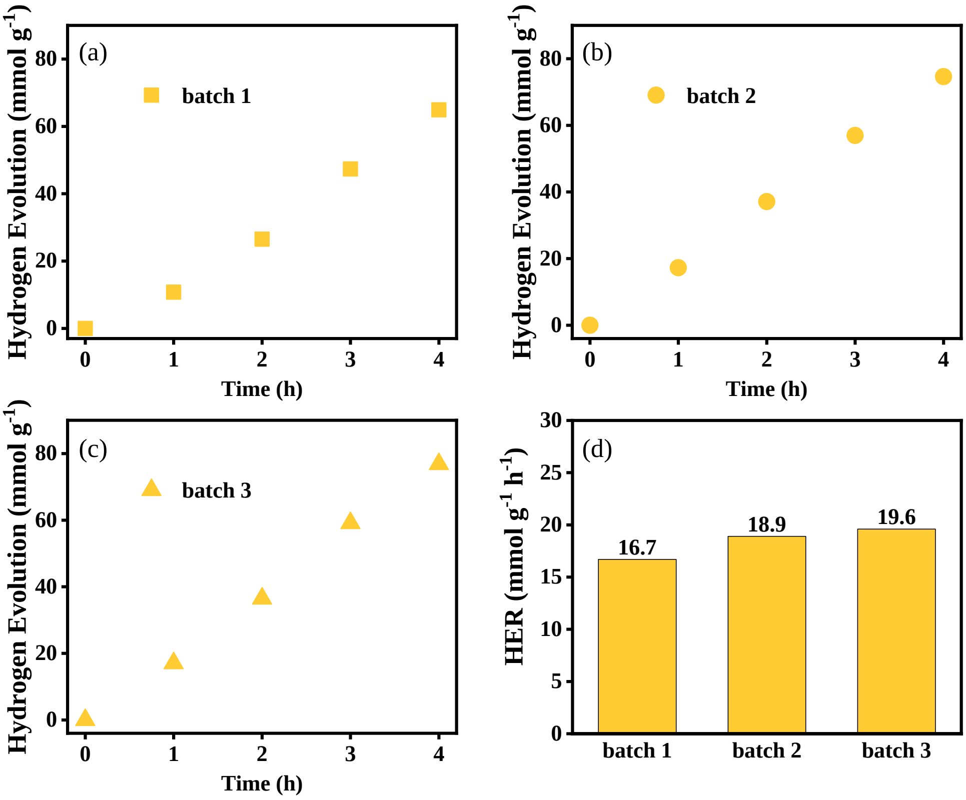

Figure S21 (a-c) Photocatalytic hydrogen production-time variation plots of **PBM** of different batches. (d) HERs of three different batches.

We prepared three batches of **PBM** using the same conditions and tested the photocatalytic hydrogen production properties. The results are 16.7, 18.9 and 19.6 mmol g^{-1} h^{-1}, respectively (Figure S21). The obtained results are very similar, implying a good reproducibility of prepared photocatalysts.

Table S9 The conjugated polymers containing B←N bonds are currently reported in the field of photocatalytic hydrogen production.

Name	Polymer structure	HERs (mmol g^{-1} h^{-1})	Reference
PBN	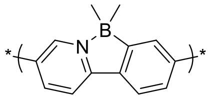	22.4	*Small*, 2023, 2302384
PBC	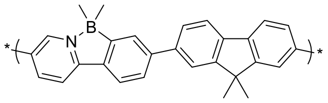	3.1	
PNBN	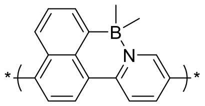	35.4	*Adv. Sci.*, 2022, **9**, 2204055
PBNP	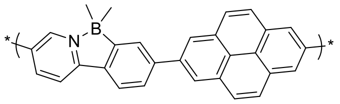	9.4	*Macromolecules*, 2023, **56**, 858-866
PBNN	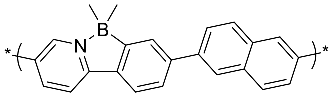	5.7	
1DPBN-2F	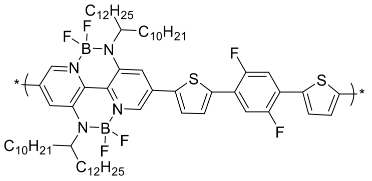	3.0	*Small Methods*, 2023, 2300409
1DPBN-4F	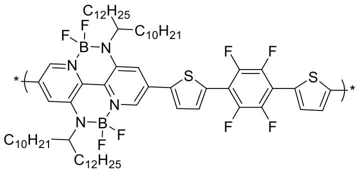	6.2	
2DPBN-2F	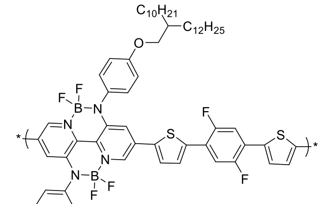	9.3	
2DPBN-4F	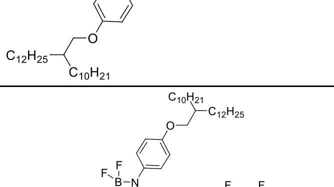	10.2	

PBM	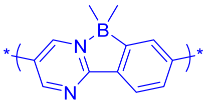	**68.8**	**This work**
PBMP	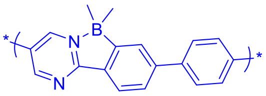	**36.3**	

Table S10 Some reported photocatalytic properties of organic polymers.

Polymers	HER (mmol g^{-1} h^{-1})	AQY (420 nm)	Reference
PBMP	28.8	9.55%	This work
PBM	18.9	6.57%	This work
PBM	68.8	-	This work
B-BT-1,4	2.3	4.01%	*Angew. Chem. Int. Ed.*, 2016, **55**, 9202-9206
PS-5	8.9	0.9%	*Sci. China Chem.*, 2022, **65**, 170-181
P7	3.7	7.2%	*Angew. Chem. Int. Ed.,* 2016, **55**, 1792-1796
CNU	15.4	4.3%	*ACS Catal.*, 2016, **6**, 3921-3931
BBT-FC8O5	10.4	2.5%	*Appl. Surf. Sci.*, 2020, **499**, 143865
Flu-SO	5.0	2.13%	*Small*, 2018, **14**, 1801839
P10	3.3	11.6%	*Nat. Commun.*, 2018, **9**, 4968
FSO-FS	3.4	6.8%	*Angew. Chem. Int. Ed.,* 2019*,* **58***,* 10236-10240
P-FSO	8.0	8.5%	*Appl. Catal. B,* 2019, **245**, 596–603
FS-TEG	2.9	10.0%	*Energy Environ. Sci.*, 2020, **13**, 1843-1855
PyDTDO-3	16.3	3.7%	*Chem. Sci.*, 2021, **12**, 1796-1802
P10-e	14.5	5.8%	*J. Mater. Chem. A*, 2019*,* **7***,* 2490-2496

Table S11 Cartesian coordinates of **M29**.

M29	x	y	z
C	3.47002073	0.00000000	0.00000001
C	2.73239072	-1.17923030	-0.00000011
C	0.77916147	0.00000000	-0.00000011
N	1.40141740	1.19106570	0.00000030
C	2.73239071	1.17923030	0.00000018
C	-0.70530242	0.00000000	-0.00000013
C	-1.41484544	1.20839399	-0.00000018
C	-1.41484545	-1.20839399	0.00000013
C	-2.80526608	-1.20606245	0.00000029
C	-3.50485902	0.00000000	-0.00000001
C	-2.80526607	1.20606245	-0.00000018
H	4.55227603	0.00000000	-0.00000008
H	3.22295378	-2.14956393	-0.00000042
H	3.22295377	2.14956393	0.00000057
H	-0.86013767	-2.13737796	0.00000030
H	-3.34490169	-2.14667264	0.00000051
H	-3.34490168	2.14667264	-0.00000030
H	-4.58942334	0.00000000	0.00000003
N	1.40141740	-1.19106570	-0.00000024
H	-0.86013767	2.13737796	-0.00000035

Table S12 Cartesian coordinates of **MBM**.

MBM	x	y	z
C	-3.35531040	-0.59296719	-0.00042375
C	-2.72286400	-1.83828993	0.00015131
C	-0.67037660	-0.86730016	0.00008228
N	-1.21123201	0.38677172	-0.00019060
C	-2.53747781	0.52492299	-0.00047010
C	0.77781592	-0.79982870	-0.00001304
C	1.20577845	0.54378670	-0.00017756
B	-0.04876900	1.55903834	0.00012183
C	1.65736931	-1.88824088	0.00008143
C	3.01903246	-1.62524569	-0.00011600
C	3.47586065	-0.29920089	-0.00046520
C	2.58451076	0.77226808	-0.00049406
C	-0.21043725	2.43385559	-1.36126673
C	-0.20970515	2.43231800	1.36259732
H	-4.43249092	-0.50145357	-0.00077062
H	-3.30663470	-2.75458097	0.00008468
H	-2.91987973	1.53865021	-0.00089627
H	1.27389126	-2.90194931	0.00036914
H	3.73202700	-2.44175085	-0.00000784
H	2.97062260	1.78684797	-0.00081792
H	-0.17569361	1.8290055	-2.27460835
H	-1.1434836	3.01224289	-1.38053151
H	0.60527371	3.16230312	-1.43143263
H	0.60650052	3.1601953	1.43313315
H	-1.14243058	3.01114267	1.38306338
H	-0.17472797	1.82640802	2.27523327
H	4.54430526	-0.10852318	-0.00077199
N	-1.39999833	-1.98537131	0.00025189

Table S13 Cartesian coordinates of **MBMP**.

MBMP	x	y	z
C	-5.17066487	-0.48295955	-0.03529405
C	-4.58230788	-1.74154562	-0.18066369
C	-2.49698104	-0.84764542	-0.09057307
N	-2.99353423	0.41704219	0.05561226
C	-4.31398348	0.59920720	0.08262970
C	-1.04964677	-0.82978660	-0.09532103
C	-0.57178562	0.48865125	0.04766131
B	-1.78964777	1.54126270	0.17489830
C	-0.20105794	-1.93508567	-0.21675151
C	1.16561518	-1.71834465	-0.19416482
C	1.69146289	-0.41535162	-0.05263904
C	0.81013260	0.67059248	0.06648285
C	-1.93014990	2.56665931	-1.07958419
C	-1.90885550	2.26219801	1.62728730
H	-6.24392344	-0.35503221	-0.01558821
H	-5.19814951	-2.63124937	-0.27851664
H	-4.66126907	1.61887073	0.19874464
H	-0.61127111	-2.93145686	-0.33399627
H	1.84467878	-2.55425614	-0.31324241
H	1.22172544	1.66556341	0.20204090
H	-1.91679638	2.06704285	-2.05502809
H	-2.84627125	3.16951213	-1.02754357
H	-1.09434492	3.27554236	-1.07345295
H	-1.06390838	2.94512929	1.77099586
H	-2.81778379	2.87088032	1.72128031
H	-1.89316262	1.55700599	2.46616821
N	-3.26576353	-1.9333179	-0.20953728
C	4.01006124	-1.09117908	0.64511389
C	5.38622169	-0.88685316	0.66911142
C	5.94497624	0.20808573	0.01308781
C	5.11446575	1.0979894	-0.66508865
C	3.73804404	0.89587866	-0.68583988
C	3.16043107	-0.20275545	-0.03138664
H	3.58492145	-1.93317827	1.17938072
H	6.02256384	-1.58043256	1.20762086
H	7.01732816	0.36644109	0.03038371
H	5.53972008	1.94885857	-1.18575936
H	3.10339979	1.58184382	-1.23491046